Cooperative regulation of AJM-1 controls junctional integrity in *Caenorhabditis elegans* epithelia

Mathias Köppen*, Jeffrey S. Simske†, Paul A. Sims†, Bonnie L. Firestein‡, David H. Hall§, Anthony D. Radice¶, Christopher Rongo# and Jeffrey D. Hardin*†**

*Program in Cellular and Molecular Biology, University of Wisconsin-Madison, 1117 West Johnson Street, Madison, Wisconsin 53706, USA
†Department of Zoology, University of Wisconsin-Madison, 1117 West Johnson Street, Madison, Wisconsin 53706, USA
‡Department of Cell Biology and Neuroscience, Rutgers University, Piscataway, New Jersey 08854, USA
§Center for C. elegans Anatomy, Department of Neuroscience, Albert Einstein College of Medicine, 1410 Pelham Parkway, Bronx, New York 10461, USA
¶Department of Stem Cell Biology, Lindsley F. Kimball Research Institute, New York Blood Center, 310 East 67th Street, New York, New York 10021, USA
#Department of Genetics, The Waksman Institute, Rutgers University, Piscataway, New Jersey 08854, USA
**e-mail: jdhardin@facstaff.wisc.edu

The function of epithelial cell sheets depends on the integrity of specialized cell–cell junctions that connect neighbouring cells. We have characterized the novel coiled-coil protein AJM-1, which localizes to an apical junctional domain of *Caenorhabditis elegans* epithelia basal to the HMR–HMP (cadherin–catenin) complex. In the absence of AJM-1, the integrity of this domain is compromised. Proper AJM-1 localization requires LET-413 and DLG-1, homologues of the *Drosophila* tumour suppressors Scribble and Discs large, respectively. DLG-1 physically interacts with AJM-1 and is required for its normal apical distribution, and LET-413 mediates the rapid accumulation of both DLG-1 and AJM-1 in the apical domain. In the absence of both *dlg-1* and *let-413* function AJM-1 is almost completely lost from apical junctions in embryos, whereas HMP-1 (α-catenin) localization is only mildly affected. We conclude that LET-413 and DLG-1 cooperatively control AJM-1 localization and that AJM-1 controls the integrity of a distinct apical junctional domain in *C. elegans*.

During animal development, specialized junctional domains are crucial for the function of epithelial cell sheets. In both vertebrates and invertebrates, adherens junctions are thought to regulate cell–cell adhesion and dynamic changes in cell morphology[1,2]. Vertebrate tight junctions and invertebrate septate junctions have been implicated in controlling the apicobasal polarity of epithelial cells (the 'fence' function) as well as regulating the passage of fluids and solutes through the paracellular space (the 'gate' function)[3–5].

Recently, proteins that regulate the polarity and junctional integrity of epithelia have been characterized. *Drosophila* Discs large, a member of the protein family of membrane-associated guanylate kinases (MAGUKs), localizes to and maintains septate junctions[6,7]. Furthermore, Discs large and the LAP4 (for 'leucine-rich repeats and four PDZ domains') protein Scribble localize together at septate junctions and act in a common pathway with the cortical protein Lethal giant larvae in controlling the localization of apical and adherens junction proteins and in regulating cell proliferation[8]. Similarly, the *Caenorhabditis elegans* LAP1 protein LET-413 localizes to basolateral domains of epithelia and has been shown to be crucial for adherens junction assembly and for the localization of apical proteins[9]. Among the junctional components whose localization is affected in *dlg* and *scrb* mutants in *Drosophila* are proteins specifically required for the gate function of septate junctions such as Neurexin IV and Band 4.1-Coracle[6,10–12]. However, the proper localization of these and other junctional components probably requires normal epithelial polarity, which is lost in *dlg* and *scrb* mutants. Therefore, a specific role for Scribble and Discs large in regulating proteins directly required to maintain the integrity of junctional domains has been difficult to demonstrate.

Here we show that the novel coiled-coil protein AJM-1 (for 'apical junction molecule') is required for the integrity of epithelial junctions of *C. elegans* and that it localizes to an apical junctional domain. (AJM-1 was originally called JAM-1 (refs 13, 14) but has been renamed to avoid confusion with the vertebrate transmembrane tight junction protein, JAM-1.) This domain is basal to the HMR–HMP(cadherin–catenin) complex; on the basis of the localization of the Discs large homologue DLG-1 to the same domain, it might be required for maintaining a tight apical seal between epithelial cells at apical junctions. Furthermore, we show that AJM-1 directly binds DLG-1, which is required for the proper distribution of AJM-1 around the junctional belt but not for general cell polarity. In addition, we show that in embryos lacking LET-413 the patterns of both DLG-1 and AJM-1 are equally disrupted, including a delay in concentration of these proteins at a narrow apical domain. Almost complete loss of junctional AJM-1 is observed in the absence of both LET-413 and DLG-1, whereas HMP-1 (α-catenin) localization is reduced but junctional. We propose a model in which LET-413 and DLG-1 control the integrity of a distinct apical subdomain by cooperatively regulating the localization of AJM-1.

Results

AJM-1 encodes a novel coiled-coil protein localizing to *C. elegans* apical junctions. As an initial step in understanding the molecular composition of apical junctions in *C. elegans*, we characterized the antigen recognized by the MH27 antibody. The antibody had been previously shown to stain apical borders of *C. elegans* epithelia[15,16]. We named the antigen AJM-1 and identified the *ajm-1* gene by probing a *C. elegans* expression library with the MH27 antibody. One complementary DNA (cDNA), mh-1, was identified; sequencing revealed that *ajm-1* corresponds to the predicted gene C25A11.4, which spans the genomic clones H08J11 and C25A11 (Fig. 1a). The *ajm-1* transcript was analysed by reverse-transcriptase-mediated polymerase chain reaction (RT–PCR), northern blot analysis and sequencing of expressed sequence tags (ESTs) from the *C. elegans* cDNA project. Five conceptual splice forms were identified. A
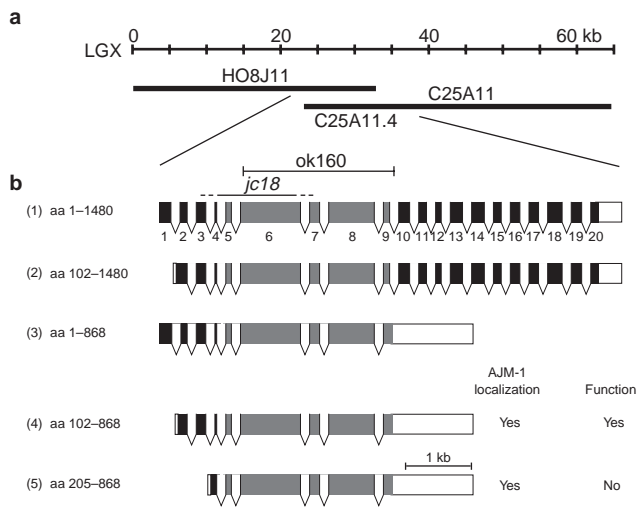
Figure 1 **ajm-1 encodes a novel coiled-coil protein. a**, *ajm-1* maps to the centre of LGX and corresponds to the predicted gene C25A11.4, which is covered by the cosmids H08J11 and C25A11. **b**, *ajm-1* splice variants. Filled boxes indicate exons; white boxes indicate 5′ and 3′ UTRs. Exons were numbered 1–20. Five conceptual splice forms encoding the amino acids (aa) indicated were deduced from the sequencing of ESTs, RT–PCR and northern blot analysis. Secondary structure analysis predicts amino acids 255–768 to form a coiled-coil motif (shown in grey). The *jc18* and *ok160* lesions are indicated. *ok160* almost completely deletes exons 6–9. *jc18* deletes exons 4–6; however, its precise 3′ and 5′ breakpoints have not been identified. Domains required for AJM-1 localization and function were determined by rescue experiments with specific splice forms (see Methods). Amino acids 102–868 were shown to be sufficient for function. Amino acids 205–868 were sufficient for junctional localization of AJM-1 (data not shown), but not for function.

BLAST search of the databases revealed no obvious homologues of AJM-1. Amino acids 255–768, which are common to all splice variants of AJM-1, are predicted to form a coiled-coil motif (Fig. 1b). Hydrophobicity analysis suggests that AJM-1 is completely hydrophilic and is therefore probably a cytoplasmic protein (data not shown). Rescue of *ajm-1* mutants was obtained with a 12-kilobase (kb) genomic fragment that encodes the two smallest splice forms; these encode amino acids 102–868 and 205–868, respectively. We therefore conclude that amino acids 102–868 are sufficient for AJM-1 function (Fig. 1b).

To address the requirement of specific domains of AJM-1 for localization and function of the protein, we analysed the expression pattern and rescuing ability of different green-fluorescent-protein (GFP)-tagged forms of the protein (see Methods). We observed that amino acids 205–868, encoding mainly the coiled-coil domain, are sufficient to localize AJM-1 to apical junctions, yet cannot rescue *ajm-1* mutants (Fig. 1b). This suggests that AJM-1 amino acids 102–204 are an essential domain of AJM-1 that is not required for localization.

The AJM-1 expression pattern was determined by staining with MH27 and expression of an *ajm-1::gfp* construct containing exons 2–9 and able to rescue *ajm-1* mutants. AJM-1 localizes to the apical borders of all *C. elegans* epithelia. Expression occurs in the embryonic hypodermis, pharynx and intestine (Fig. 2a, b, e, f), as well as in post-embryonic epithelia, including the vulva, uterus, spermathecae (Fig. 2c, d), pharynx, intestine, hindgut, hypodermis and male tail (data not shown). MH27 staining of embryos expressing HMP-1–GFP reveals that AJM-1 occupies an apical domain that is basal to the HMR–HMP(cadherin–catenin) complex in all epithelial tissues examined (Fig. 2e, f). Transmission electron microscopy (TEM) analysis of embryonic hypodermal cell junctions revealed
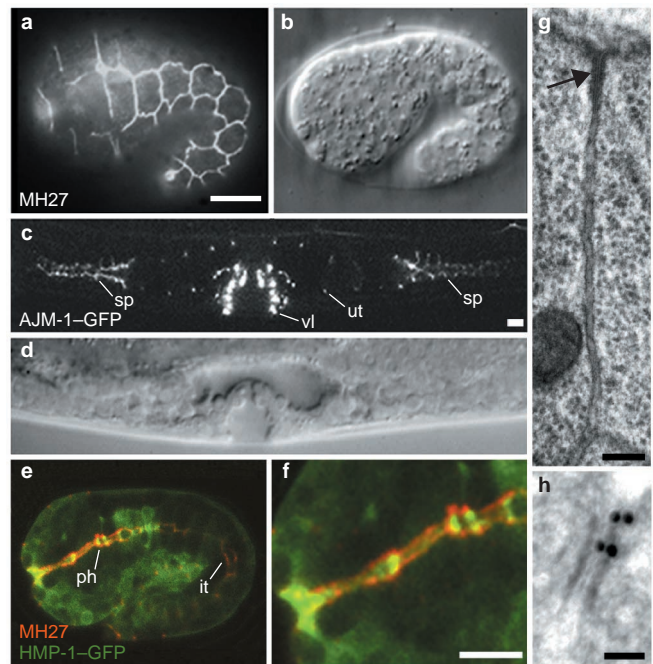

Figure 2 **AJM-1 localizes to a distinct apical domain of epithelial junctions.**
a, **b**, Embryonic AJM-1 expression. Embryos in this and all subsequent figures are presented with anterior to the left and dorsal at the top. **a**, MH27 staining outlines the apical borders of hypodermal cells. **b**, A Nomarski image of a comparable embryo. **c**, **d**, AJM-1 expression in larval epithelia. **c**, AJM-1–GFP localization to apical cell borders of the spermathecae (sp), vulva (vl) and uterus (ut) of an L4 larva. **d**, A Nomarski image of the same animal. **e**, **f**, Comparison of the MH27 (in red) and HMP-1–GFP (in green) patterns in an embryo. **e**, Both markers outline the apical borders of the pharynx (ph) and the intestine (it). **f**, Magnification of the pharynx region reveals that HMP-1–GFP is closer to the lumen and is flanked by MH27, indicating that MH27 stains a more basal domain. The same relative positions of AJM-1 and HMP-1 were also observed in the hypodermis (data not shown). **g**, A TEM image of a hypodermal cell junction of a wild-type embryo. An electron-dense apical domain (arrow) links the cells, and clearly defined septae in the junction are not present. **h**, Immunogold labelling with MH27 reveals specific labelling at the apical junction. Scale bars, 10 μm (**a**,**c**), 5 μm (**f**),100 nm (**g**) and 50 nm (**h**).

an apical junctional domain resembling adherens junctions of flies and vertebrates, whereas no morphologically distinct septate or tight junctions are observed. The apicobasal extent of this domain is ~100 nm (Fig. 2g). Immuno-TEM analysis of hypodermal cells of larvae with the MH27 antibody revealed that AJM-1 specifically localizes to the apical domain (Fig. 2h).

ajm-1 mutant embryos are arrested during late embryonic elongation. To address the function of AJM-1, we generated *ajm-1* mutant alleles. *ajm-1(jc18)* was isolated in a linked-lethal screen and *ajm-1(ok160)* in a PCR-based screen (data not shown). *ok160* deletes almost the entire predicted coiled-coil domain. *jc18* deletes exons 4–6, although the precise 3′ and 5′ breakpoints are unidentified (Fig. 1b). Both alleles are predicted nulls and show the same phenotype as *ajm-1(RNAi)* embryos (data not shown). *ok160* was used for all subsequent analysis.

During wild-type embryogenesis, the animal is enclosed by an epithelial sheet (hypodermis) and subsequently elongates to about four times its original length before hatching (Fig. 3a–c)[17,18]. *ajm-1* embryos enclose normally and initiate elongation without obvious morphological abnormalities (Fig. 3d, e), yet at a slower rate than the wild type. Wild-type embryos reach the 2-fold stage 90 ± 0.4 min (mean ± SEM, $n = 12$) after completion of enclosure, whereas *ajm-1* embryos require 124 ± 3.8 min ($n = 13$). In *ajm-1* embryos,
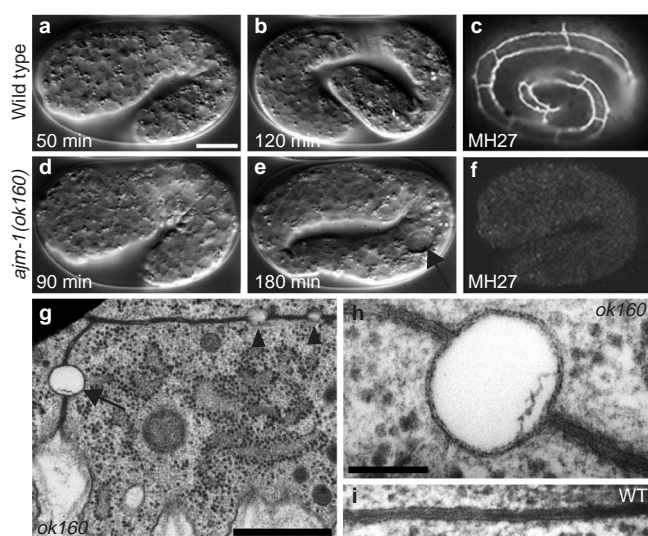
Figure 3 *ajm-1(ok160)* embryos are arrested at the twofold stage and display compromised integrity of apical junctions. **a–c**, Wild-type embryos. Two time points of a time-lapse recording show that during elongation the wild-type embryo reaches the 1.5-fold stage ~50 min after completion of enclosure (**a**), and the 3-fold stage is reached ~120 min after enclosure (**b**). MH27 staining shows the typical junctional pattern (**c**). **d–f**, *ajm-1(ok160)* embryos. The embryo reaches the 1.5-fold stage without apparent morphological abnormalities, yet is significantly delayed, reaching 1.5-fold 90 min after enclosure (**d**). After reaching the 2-fold stage at ~130 min after enclosure (data not shown) elongation stops and a large vacuole forms in the body cavity near the posterior end of the actively twitching embryo (arrow) (**e**), followed by developmental arrest. MH27 staining is completely abolished in *ajm-1(ok160)* embryos (**f**). **g–i**, TEM analysis of apical junctions of an *ajm-1(ok160)* embryo and a wild-type embryo. (**g**) A glancing section through the apical surface of a hypodermal cell of an *ajm-1(ok160)* embryo, permitting the assessment of junctional integrity along the entire cell border. As is consistently observed in *ajm-1(ok160)* embryos, separations within the apical junction are visible (arrowheads and arrow). A higher magnification of the largest separation (arrow) reveals that the junction is evenly split open, creating a paracellular gap of 190 nm in width (**h**). The junctional areas flanking the separation seem properly sealed and ~15 nm wide, as in the wild-type (WT) junction in (**i**), with paracellular gaps ranging between 0 and 2 nm. Scale bars, 10 μm (**a**), 0.5 μm (**g**) and 100 nm (**h**).

elongation is consistently arrested at the 2–3-fold stage, accompanied by the formation of a large vacuole in the posterior region (Fig. 3e). *ajm-1* embryos lack MH27 staining (Fig. 3f). We conclude that AJM-1 is required for the correct rate and completion of elongation of the *C. elegans* embryo.

The process of embryonic elongation has been shown to depend on the HMR–HMP(cadherin–catenin) complex, which mediates the junctional attachment of circumferential microfilaments providing the contractile force that is thought to drive elongation[17,19]. In addition, elongation past the 2-fold stage depends on the proper attachment of body wall muscle to the hypodermis[20,21]. We therefore analysed *ajm-1* embryos for possible defects in the integrity of the HMR–HMP complex, microfilament alignment and the pattern of body wall muscle. Mutants for components of the HMR–HMP complex typically display incomplete enclosure or severe defects during initial elongation, but show unaltered AJM-1 localization[14,19]. We analysed the pattern of HMP-1 (α-catenin) in *ajm-1* mutants by using HMP-1–GFP and anti-HMP-1 expression and observed patterns identical to the wild type in both cases. Furthermore, *ajm-1* embryos display a normal alignment of circumferential microfilaments (data not shown). We analysed the pattern and function of body wall muscle in *ajm-1* embryos by

using the muscle-specific antibody R224 (ref. 22) and observed a wild-type pattern. In addition, *ajm-1* embryos begin twitching at around 1.75-fold stage (data not shown), indicating wild-type muscle activity[23]. These results suggest that AJM-1 and the HMR–HMP complex localize and function mutually independently. Furthermore, AJM-1 is not required for the circumferential alignment of microfilaments and for the positioning and function of body wall muscle in the embryo.

AJM-1 is required for junctional integrity but not epithelial polarity. To address the functional role of AJM-1 in apical junctions specifically, we analysed *ajm-1* embryos at the ultrastructural level by TEM. Apical junctions of *C. elegans* epithelia appear as a continuous close apposition of neighbouring cells. They contain electron-dense material at the cytoplasmic face of the membranes and an electron-dense area in the paracellular space (Fig. 2g and Fig. 3g–i). Thin sections of hypodermal cells of *ajm-1* embryos display apical junctions that are properly positioned (data not shown). However, the close apposition of these junctions is disrupted intermittently by ring-shaped separations along the whole length of the junctional belt. These separations create paracellular gaps that are typically between 50 and 200 nm in diameter, whereas properly sealed domains are ~15 nm wide with paracellular gaps of 0–2 nm (Fig. 3g–i). Analysis of serial thin sections revealed that the apical–basal extent of the separations is ~100 nm and that they comprise only the electron-dense apical domain. Close membrane apposition is observed both apical to and basal to the separations (data not shown). We conclude that AJM-1 is required for maintaining the integrity of the electron-dense domain of apical junctions.

To address further whether AJM-1 is required for epithelial polarity, we analysed the localization of apical and basal markers in *ajm-1* embryos. As apical markers we used antibodies against SMA-1 (βH-spectrin), which localizes apically in hypodermal cells (J. Austin, personal communication), and PAR-3 and PAR-6, which localize apically of AJM-1 in the pharynx and intestine (data not shown). Antibodies against UNC-70 (βG-spectrin) were used as a basolateral marker in the hypodermis[24], and as basal markers we used the monoclonal antibodies MH46 and MH5, which recognize components of hemidesmosomes involved in body wall muscle attachment[25]. In each case, protein localization was unaltered in *ajm-1* embryos in comparison with the wild type (data not shown). This suggests that AJM-1 is not required for epithelial polarity.

AJM-1 and DLG-1 physically interact and function in a common pathway. To identify proteins that are required for AJM-1 localization and function, we performed a yeast two-hybrid screen with a fusion protein between AJM-1 and the DNA-binding domain of LexA as bait. The pLexA–AJM-1 construct was made with a partial *ajm-1* cDNA encoding amino acids 180–809 of the protein, which include the predicted coiled-coil domain. Of the 200,000 transformants screened, two independently isolated cDNAs were found corresponding to the *dlg-1* gene. *dlg-1* encodes the *C. elegans* homologue of *Drosophila* Discs large (Fig. 4a)[26,27]. Both *dlg-1* cDNAs isolated in the two-hybrid assay encode amino acids 28–483 of the predicted DLG-1 protein. To confirm this interaction in an independent assay, we performed an *in vitro* pull-down experiment with a fusion of glutathione *S*-transferase (GST) and DLG-1 (amino acids 28–483). Full-length ^{35}S-labelled AJM-1 (amino acids 1–868) was produced by translation *in vitro* and incubated with beads carrying GST–DLG-1 or GST. Radiolabelled AJM-1 bound to GST–DLG-1 but not to GST alone (Fig. 4b).

DLG-1 is a member of the family of membrane-associated guanylate kinases, containing three PDZ domains, an SH3 domain and a guanylate kinase domain. Amino acids 28–483 of the protein contain the first two PDZ domains (amino acids 210–289 and 369–448) and additional residues amino-terminal and carboxy-terminal to those domains (Fig. 4c). PDZ domains have been previously implicated in protein–protein interaction in *Drosophila* Discs large and other MAGUK proteins[7,28]. PDZ domains of Discs large-like MAGUKs favour binding partners with a C-terminal E(S/T)X(V/I) domain
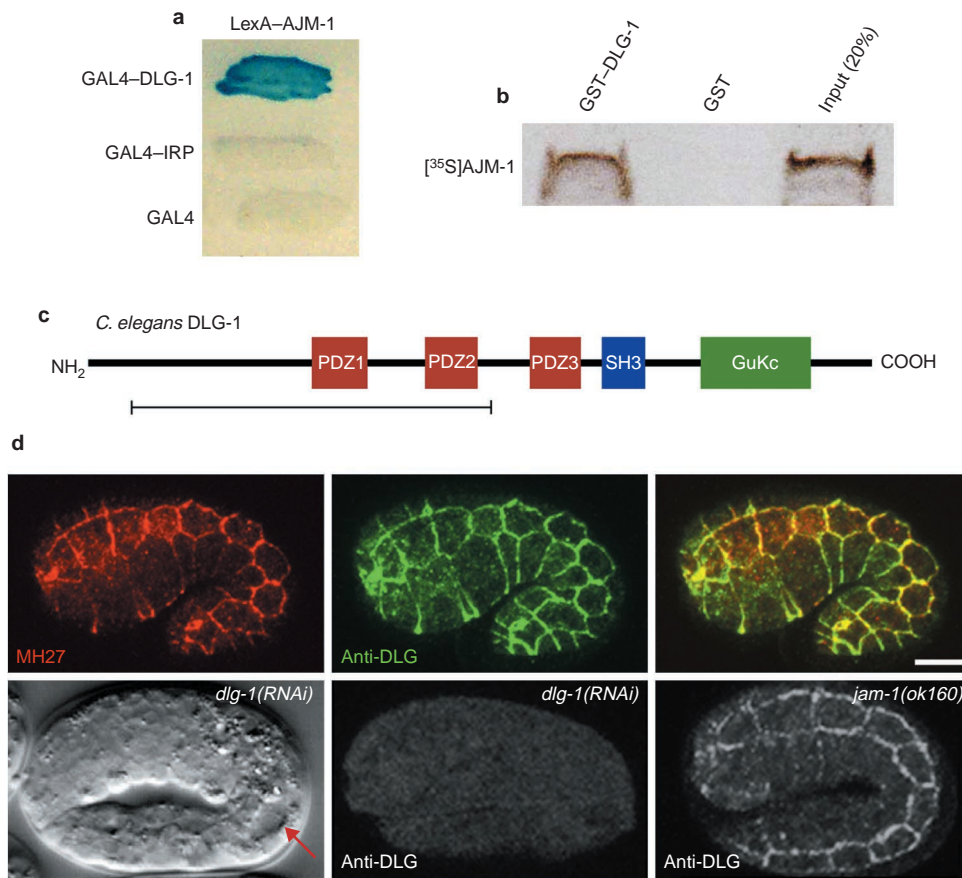
Figure 4 **AJM-1 and DLG-1 physically interact and function in a common pathway. a**, AJM-1–DLG-1 interaction in yeast. An unbiased yeast two-hybrid screen was conducted with AJM-1 (amino acids 180–809) fused to the LexA DNA-binding domain as bait. Two independently isolated cDNAs correspond to *dlg-1*. Specificity of the AJM-1–DLG-1 interaction was confirmed in directed interaction tests with yeast containing the pLexA–AJM-1 plasmid and either the identified cDNAs or control plasmids. β-Galactosidase acitivity was detected in yeast expressing the Gal4 activation domain–DLG-1 fusion protein (Gal4–DLG-1) and LexA–AJM-1 (top streak). Control assays using Gal4–IRP (iron response protein) or Gal4 resulted in a complete lack of β-galactosidase activity (middle and bottom streaks, respectively). **b**, AJM-1–DLG-1 interaction *in vitro*. Sepharose beads carrying a GST–DLG-1 fusion protein (amino acids 28–483 of DLG-1) or GST were incubated with radiolabelled AJM-1 (amino acids 1–868). Bound protein was eluted and analysed by SDS–PAGE. Binding was observed between AJM-1 and GST–DLG-1 (left lane) but not between AJM-1 and GST alone (middle lane). The right lane shows labelled AJM-1 protein equivalent to 20% of the material analysed in the experimental lanes. **c**, DLG-1 domain structure. The *dlg-1* encodes a 967-amino-acid protein, containing three PDZ domains, an SH3 domain and a GuKc domain. The bar indicates the region encoded by both cDNAs identified in the yeast two-hybrid screen (amino acids 28–483). **d**, DLG-1 localization and *dlg-1(RNAi)* phenotype. A wild-type embryo was immunostained with MH27 and anti-DLG antibodies raised against *Drosophila* Discs large[31]. The upper left panel shows MH27 staining in hypodermal cells. The upper middle panel shows anti-DLG in the same focal plane. Both patterns overlap completely in a merged image (upper right panel). Analysis of a *dlg-1(RNAi)* embryo with Nomarski video-microscopy reveals a phenotype similar to that of *ajm-1* embryos. The embryo is arrested at around the 2-fold stage of elongation and forms a large vacuole in the posterior body cavity (arrow, bottom left panel). A *dlg-1(RNAi)* embryo stained with anti-DLG antibodies shows a complete absence of staining (bottom middle panel), whereas an *ajm-1(ok160)* embryo shows proper anti-DLG-1 staining (bottom right panel). Scale bar, 10 μm.

(single-letter amino acid abbreviations)[29]. However, this motif is not found in AJM-1. Furthermore, the AJM-1 protein used in the two-hybrid screen (but not in the GST pull-down assay) lacked the C-terminal 59 amino acids. This suggests that the interaction with DLG-1 does not involve the C terminus of AJM-1. Similarly, the coiled-coil protein cingulin has been shown to interact with the MAGUK proteins ZO-1, ZO-2 and ZO-3 through its N-terminal domain[30]. We propose that AJM-1 either contains a novel internal PDZ-interaction domain, or alternatively that the interaction does not involve the PDZ domains. Additional structure–function analyses will address these possibilities.

To analyse the expression pattern of DLG-1 in *C. elegans* embryos, we stained embryos with a polyclonal antibody raised against the highly conserved amino acids 39–251 of *Drosophila* Discs large[31]. Consistent with another report that was published while this work was being reviewed was our observation, by laser scanning confocal microscopy analysis, of complete co-localization with AJM-1 to the apical junctions in the hypodermis (Fig. 4d), pharynx and the intestine (data not shown)[27]. We conclude that AJM-1 and DLG-1 physically interact at apical junctions.

We addressed the function of DLG-1 protein by using RNA-mediated interference (RNAi)[32]. At the level of Nomarksi microscopy, *dlg-1(RNAi)* embryos display an arrest phenotype that is morphologically similar to, but slightly more severe than, that of *ajm-1* embryos. Elongation is arrested immediately before or at the 2-fold stage at ~165 ± 6.7 min (mean ± SEM, $n = 6$) after the initiation of elongation (Fig. 4d and data not shown). Therefore, the elongation of *dlg-1(RNAi)* embryos is significantly slower than that of both wild-type and *ajm-1* mutants. Like *ajm-1* mutants, *dlg-1(RNAi)* embryos typically display a large vacuole in the posterior
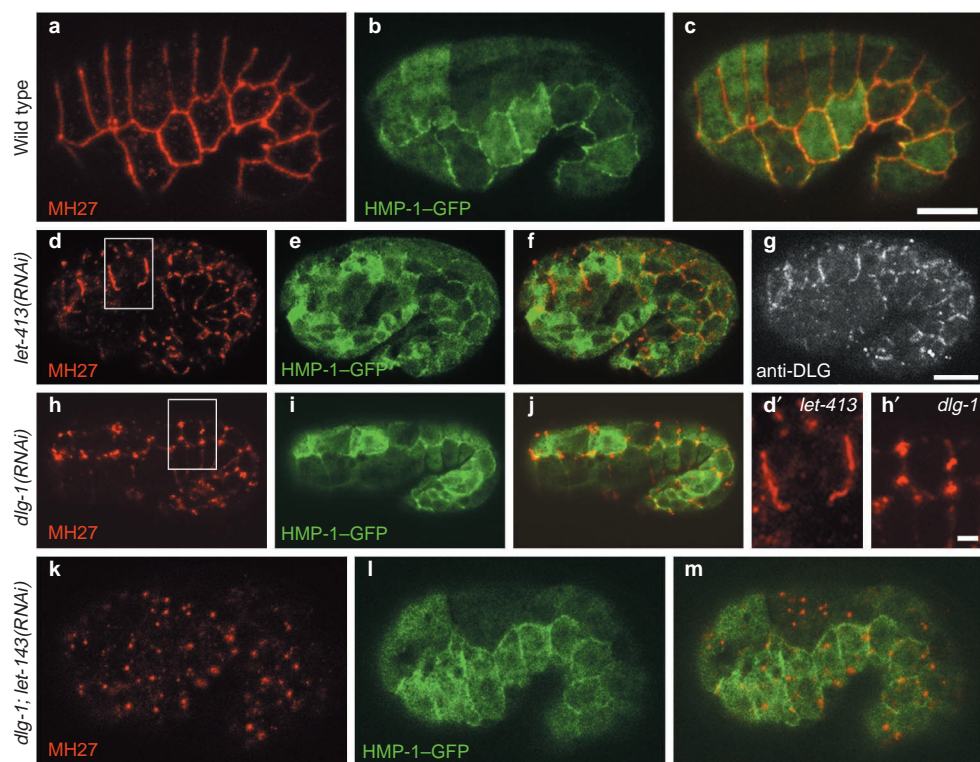
Figure 5 **LET-413 and DLG-1 cooperatively control AJM-1 localization.**
Comparison of the MH27 and HMP-1–GFP patterns in wild-type, *dlg-1(RNAi)*, *let-413(RNAi)* and *dlg-1;let-413(RNAi)* embryos with confocal microscopy. **a–c**, Wild type. MH27 (**a**) and HMP-1–GFP (**b**) show continuous junctional localization and the merged image reveals that both patterns are closely associated (**c**). **d–g**, *let-413(RNAi)*. The MH27 pattern reveals long stretches of normal AJM-1 localization that are separated intermittently by gaps completely lacking AJM-1 (**d**); a magnification of the boxed area is shown in (**d′**). Junctional HMP-1–GFP is observed but is reduced compared with the wild type (**e**). Adjacent localization of the MH27 signal and HMP-1–GFP is maintained, as observed in the merged image (**f**). Anti-DLG stain- ing of the same embryo reveals a pattern that is largely identical to the MH27 pattern (**g**). **h–j**, *dlg-1(RNAi)*. The MH27 pattern is characterized by aggregates sepa- rated by large regions in which MH27 staining is greatly reduced (**h**); a magnifica- tion of the boxed area is shown in (**h′**). The HMP-1–GFP pattern is unaltered com- pared with the wild type (**i**), and the remaining MH27 signal is closely associated with HMP-1–GFP (**j**). **k–m**, *let-413; dlg-1(RNAi)*. Junctional MH27 staining is com- pletely abolished (**k**), whereas the HMP-1–GFP pattern is similar to that in *let-413(RNAi)* embryos (**l**). In the merged image no significant overlap of MH27 and HMP-1–GFP is observed (**m**). Scale bars, 10 μm (**c, g**) and 2 μm (**h′**).

region (Fig. 4d). We observed no anti-DLG-1 staining in *dlg-1(RNAi)* embryos, confirming that the antibody recognizes DLG-1. *ajm-1* mutant embryos display a DLG-1 expression pattern that is identical to the wild type (Fig. 4d). Next, we eliminated *dlg-1* func- tion in *ajm-1* embryos. The phenotype observed was identical to that of *dlg-1(RNAi)* embryos with respect to the stage of embryon- ic arrest, the morphology of the embryos and the rate of elongation (data not shown). Taken together, these results indicate that DLG- 1 is required for proper embryonic elongation; DLG-1 probably acts upstream of AJM-1 and becomes localized to apical junctions independently of AJM-1.

LET-413 and DLG-1 cooperatively regulate AJM-1 localization. LET- 413 is a LAP1 protein, containing leucine-rich repeats and one PDZ domain. LET-413 is localized to the basolateral domains of epithelial cell membranes, and in *let-413* mutant embryos apical junctions dis- play severe structural defects. In addition, the localization of apical proteins, including AJM-1, is disrupted[9]. AJM-1 mislocalization in *dlg-1(RNAi)* embryos has also been described[27]. To explain in more detail how AJM-1 localization is regulated by LET-413 and DLG-1, we carefully compared AJM-1 localization in embryos lacking either LET-413 or DLG-1, or both.

Our results confirm that *let-413(RNAi)*, *let-413(s128)* and *sDf35* embryos (the deficiency deleting the *let-413* gene) consistently rup- ture after the 1.5-fold stage of elongation (data not shown)[9]. We analysed AJM-1 localization in these three backgrounds and obtained identical results for each. We observed an AJM-1 pattern showing regions of normal localization separated by intermittent gaps (Fig. 5d, d′). In *let-413(RNAi)* embryos, junctional localiza- tion of HMP-1–GFP is observed consistently, although at lower lev- els than in wild-type embryos (Fig. 5b, e). Similar results were obtained from immunostaining of *let-413(RNAi)* embryos and *let-413(s128)* mutants with anti-HMP-1 (data not shown). The remaining AJM-1 protein is closely associated with HMP-1–GFP, suggesting that it is localized to apical junctions as in the wild type (Fig. 5c, f). We next compared DLG-1 and AJM-1 localization in *let-413(RNAi)* embryos. Invariably, the patterns of both proteins are identical and completely overlap in merged images (Fig. 5d, g and data not shown). *dlg-1(RNAi)* embryos consistently show an AJM-1 mislocalization pattern that is distinct from that in *let-413(RNAi)* embryos: AJM-1 localizes to apical junctions, but unlike the even, uninterrupted AJM-1 pattern of wild-type embryos, we observe regions of AJM-1 aggregation that alternate with large regions in which AJM-1 expression is greatly reduced; this pattern is reminiscent of 'beads on a string' (Fig. 5a, h, h′). The HMP-1–GFP pattern in these embryos is unaltered, and AJM-1 remains closely adjacent to HMP-1–GFP at apical junctions (Fig. 5i, j). In embryos deprived of both LET-413 and DLG-1 by RNAi, the junc- tional localization of AJM-1 is almost completely abolished. HMP-1–GFP shows reduced expression but remains junctional (Fig. 5k–m). Taken together, these results suggest that LET-413 and
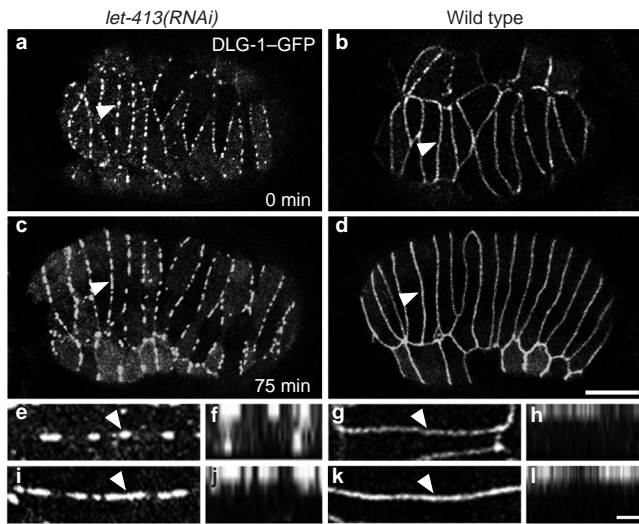
Fig. 6 **LET-413 is required for rapid apical confinement of DLG-1.** Dynamic analyses of DLG-1-GFP expression in a developing *let-413(RNAi)* and wild-type embryo were performed with time-lapse multiphoton laser scanning microscopy. DLG-1-GFP distribution along individual apical junctions was correlated with apicobasal distribution of the protein over time. During early epithelial morphogenesis (dorsal intercalation), DLG-1-GFP shows a punctate pattern in all dorsal epithelial cells of the *let-413(RNAi)* embryo; for further analysis, one cell border is marked with an arrowhead (**a**, and enlarged in **e**). A Z-projection of the marked cell border reveals that DLG-1-GFP is localized apically as well as laterally (**f**). The equivalently staged wild-type embryo shows a completely continuous DLG-1-GFP pattern (**b**, **g**), and DLG-1-GFP is confined to a narrow apical domain within the junction (**h**). At 75 min. later, after the completion of dorsal intercalation, further DLG-1-GFP has accumulated in the apical junctions of the *let-413(RNAi)* embryo (**c**, **i**); the DLG-1-GFP pattern of the marked junction has become more similar to that of the wild-type junction (**d**, **k**). Comparison of the apicobasal distribution of DLG-GFP at this stage reveals that the protein has become confined apically within the *let-413(RNAi)* junction (**j**), similar to the wild-type junction (**l**). Scale bars represent 10 mm (**d**) and 2 mm (**l**).
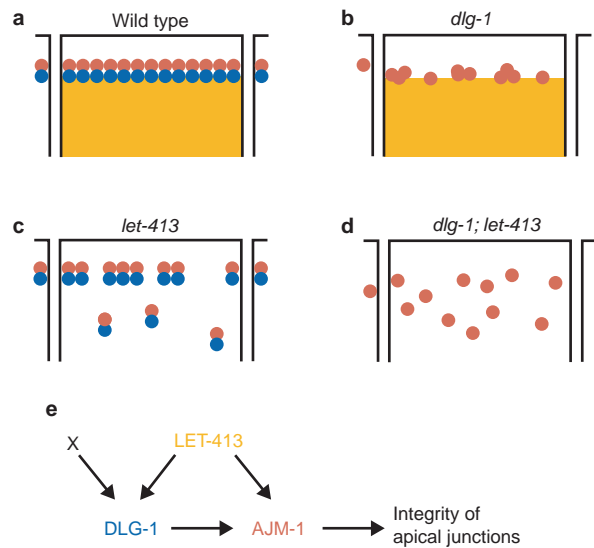

Figure 7 **Model for the control of AJM-1 localization by LET-413 and DLG-1. a**, In the wild type, AJM-1 (red) is distributed in a continuous pattern at apical junctions in the presence of LET-413 (yellow), which localizes basolaterally, and DLG-1 (blue), which binds AJM-1 at apical junctions. **b**, In the absence of DLG-1, apical AJM-1 is decreased, and in addition the protein is unevenly distributed within the apical domain. **c**, In the absence of LET-413, rapid apical confinement of DLG-1 and AJM-1 does not occur, resulting in a decrease in the apical localization of both proteins and misdistribution to the lateral domain. **d**, In the absence of both LET-413 and DLG-1, localization of AJM-1 to apical junctions is almost completely lost. The protein is randomly distributed along the apicobasal axis or lost from cell borders. **e**, A proposed pathway of AJM-1 localization. LET-413 is required for the localization of DLG-1, which directly controls AJM-1 localization. In addition, an unknown factor is required to account for the significant amount of apical DLG-1 in the absence of LET-413 (protein X; **c**). LET-413 also affects AJM-1 localization via a DLG-1-independent pathway; loss of both the DLG-1-dependent and DLG-1-independent pathways leads to a marked mislocalization of AJM-1 in the absence of both LET-413 and DLG-1 (**d**) compared with the loss of DLG-1 alone (**b**).

DLG-1 cooperatively regulate AJM-1 localization to apical junctions, whereas normal junctional localization of HMP-1 is partly dependent on LET-413 but not DLG-1.

To address how LET-413 functions in localizing DLG-1 and AJM-1 to apical junctions, we analysed the dynamics of the apicobasal distribution of DLG-1 and AJM-1 in individual hypodermal junctions of wild-type and *let-413(RNAi)* embryos over time. Time-lapse multi-photon analysis of a DLG-1–GFP fusion protein revealed that during an early phase of hypodermal morphogenesis (dorsal intercalation) in *let-413(RNAi)* embryos, DLG-1–GFP shows punctate localization to apical hypodermal junctions and is partly localized to the lateral membrane domain (Fig. 6a, e, f). In contrast, comparable wild-type embryos display a continuous pattern of DLG-1–GFP that is completely apical (Fig. 6b, g, h). As hypodermal morphogenesis proceeds, DLG-1–GFP accumulates at a narrow apical region of the hypodermal junctions of *let-413(RNAi)* embryos (Fig. 6c ,i, j), forming a pattern comparable with that of wild-type embryos (Fig. 6d, k, l). Similar results were obtained for AJM-1–GFP (data not shown). We conclude that LET-413 is required for rapid confinement of DLG-1 and AJM-1 to a narrow apical region in *C. elegans* epithelia. Apical confinement of both proteins occurs in the absence of LET-413, but more slowly.

Discussion

Our results indicate that AJM-1 is a novel coiled-coil protein that localizes to a distinct apical domain of epithelial junctions of *C. elegans* and is required for maintaining the integrity of this domain. Junctional localization of AJM-1 is regulated by both the Discs large homologue DLG-1 and the LAP1 protein LET-413. AJM-1 seems to interact directly with DLG-1 at apical junctions, whereas LET-413 mediates the rapid apical localization of both DLG-1 and AJM-1.

Analysis of AJM-1 localization by immunofluorecence and immunogold TEM reveals that AJM-1 occupies a distinct apical junctional domain in *C. elegans* epithelia that is basal to the HMR–HMP (cadherin–catenin) complex. AJM-1 is required during embryogenesis, because *ajm-1* mutant embryos are consistently arrested at the 2–3-fold stage of elongation. This phenotype clearly differs from that resulting from a compromised HMR–HMP complex. Mutants lacking any component of the complex show incomplete enclosure of the embryo by the hypodermis and subsequent rupture during elongation, as well as misalignment of microfilaments. This defect probably results from a failure to form adherens junctions between leading ventral hypodermal cells during enclosure, or from a failure to anchor properly the microfilaments that transmit contractile forces to the junctions during elongation[14,19]. In *ajm-1* embryos, no epithelial ruptures, body shape defects or improper microfilament alignment are observed. Consistent with this was the observation that AJM-1 localizes normally in the absence of the HMR–HMP complex[14,19]; here we report normal localization of HMP-1 (α-catenin) in the

absence of AJM-1. AJM-1 therefore seems to perform a function that is independent of the HMR–HMP complex, which is consistent with localization of AJM-1 to a distinct apical domain. Ultrastructural analysis of the hypodermis of *ajm-1* embryos reveals apical junctions that are properly positioned and have, in part, a normal morphology. However, whereas wild-type junctions appear as continuous close appositions between neighbouring epithelial cells, numerous small separations of the junctions are observed in *ajm-1* mutants. Apart from the apical junction to which AJM-1 localizes, we observe no morphologically distinct structures in the cell borders between epithelial cells of *C. elegans* that could be candidates for maintaining the paracellular seal. This apical junction might therefore serve as a permeability barrier. Consistent with this hypothesis is the observation that this domain is basal to the cadherin–catenin complex and contains Discs large, which is analogous to the *Drosophila* septate junction, a proposed permeability barrier[10,11]. We speculate that the junctional separations observed in *ajm-1* embryos allow the excessive passage of fluid across the hypodermis through the paracellular space, causing embryonic arrest owing to osmotic imbalance between the pseudocoelom and the exterior of the embryo. The large vacuole that consistently forms in the posterior region of elongating *ajm-1* embryos might result from the accumulation of fluid in the pseudocoelom. However, our attempts to analyse epithelial permeability of size-specific dyes in *ajm-1* embryos have so far been inconclusive (M. K., P. A. S. and J. D. H., unpublished observations). The close apposition of epithelial cells apical and basal to the junctional separations in *ajm-1* mutants might still provide a sufficient physical barrier to restrict dye movement in such experiments.

ajm-1 is predicted to encode a novel cytoplasmic protein. Several splice variants of the *ajm-1* transcript were identified. However, AJM-1 function requires only two essential domains: a short N-terminal domain without obvious secondary structure, followed by a putative coiled-coil domain. The roles of alternative N and C termini are not known. Our GFP-tagging experiments have demonstrated that the coiled-coil domain is sufficient for localizing AJM-1 to junctions. The function of the critical N-terminal domain is currently unclear. Several coiled-coil proteins with structural similarity to the coiled-coil domain of AJM-1 have been shown to bind and crosslink cytoskeletal components. These include the mammalian proteins trichohyalin, caldesmon and plectin[33–35]. In addition, recent studies have implicated coiled-coil motifs in membrane-anchored scaffolding of structural and functional proteins at the cytoplasmic face of vertebrate tight junctions. The coiled-coil-containing protein cingulin and the intracellular coiled-coil motif of occludin interact physically with other tight-junction components, including the MAGUK proteins ZO-1, ZO-2 and ZO-3, and interact directly with the actin cytoskeleton[30,36,37]. Similarly, AJM-1 might contribute to the assembly and integrity of apical junctions between epithelial cells of *C. elegans* by clustering cytoplasmic and/or transmembrane components at junctions. Testing this model will require the identification of other direct binding partners of AJM-1. A potential requirement for AJM-1 in organizing actin filaments at apical junctions was not confirmed by the use of phalloidin staining; however, a more in-depth analysis at the ultrastructural level might be necessary to address this possibility better.

Our results suggest that AJM-1 localization to apical junctions is controlled cooperatively by the MAGUK protein DLG-1 and the LAP-1 protein LET-413. We have shown that DLG-1 might be directly required for proper AJM-1 localization at apical junctions (Fig. 7a); DLG-1 and AJM-1 interact physically in yeast as well as *in vitro*, and both proteins localize together at apical junctions of *C. elegans*. Furthermore, loss of DLG-1 causes similar developmental arrest to that caused by the loss of AJM-1, and loss of both DLG-1 and AJM-1 causes a phenotype indistinguishable from that produced by the loss of DLG-1 only. This suggests that both proteins act in a common pathway. In the absence of DLG-1, the junctional

AJM-1 level is decreased and misdistributed along the junctional ring (Fig. 7b), whereas the formation and apical localization of the cadherin–catenin complex as well as general apicobasal polarity are unaffected. Thus, one way in which DLG-1 seems to control the integrity of apical junctions is by mediating the proper distribution of AJM-1 along the junctions.

LET-413 had been shown to localize to the basal and basolateral membranes of epithelial cells and to be required for the proper localization of apical proteins[9]. We have shown that DLG-1 and AJM-1 are found in the junctional belt in the absence of LET-413. However, the normally continuous distributions of DLG-1 and AJM-1 are equally disrupted by gaps, and both proteins partly mislocalize to the lateral membrane domain (Fig. 7c). Moreover, our results indicate that LET-413 mediates a rapid accumulation of DLG-1 and AJM-1 at apical junctions. An apical accumulation of both proteins occurs in the absence of LET-413 but is significantly delayed. We propose two models for how LET-413 might function in this process. Apical localization of DLG-1 and AJM-1 might involve an initial, LET-413-independent localization to the lateral membrane domain, given the lateral localization of the proteins observed in the absence of LET-413. This is followed by LET-413-dependent translocation to the apical domain. Equally plausibly, DLG-1 and AJM-1 might be targeted directly to the apical membrane domain via a currently unidentified mechanism, and LET-413 might exclude these proteins from the lateral membrane domain. Clearly, these two mechanisms are not mutually exclusive. A more temporally refined dynamic analysis of DLG-1 and AJM-1 deposition might help to distinguish between these possibilities. Significantly, we observed that the AJM-1 pattern is more severely affected in embryos lacking the functions of both LET-413 and DLG-1 than in embryos lacking the function of either protein alone (Fig. 7d). This result argues against a strictly linear pathway in which LET-413 affects AJM-1 exclusively by controlling DLG-1 localization. We propose that, in addition, LET-413 controls AJM-1 localization via a parallel pathway that is independent of DLG-1 (Fig. 7e).

Our analysis allows us to infer additional aspects of junctional regulation in *C. elegans*. Unidentified factors probably contribute to the localization of DLG-1 to apical junctions, because there is a significant amount of apical DLG-1 and AJM-1 in the absence of LET-413. That junctional localization of HMP-1 (α-catenin) is decreased in the hypodermis is consistent with a study showing a decrease in junctional HMP-1 in the gut epithelium of *let-413* mutant embryos[27], and extends these findings to the hypodermis. We did not observe the essentially cytoplasmic localization of HMP-1 in the hypodermis that had previously been reported for ~50% of *let-413* mutant embryos in an additional study[9]. Taken together, these results argue that additional apical cues exist that function in parallel with LET-413 (Fig. 7e). A more complete understanding of apical targeting of proteins awaits the identification of additional factors that complement the roles of LET-413.

Our model for the regulation of junctional integrity in *C. elegans* by LET-413, DLG-1 and AJM-1 differs significantly from the roles proposed for the LAP4 protein Scribble and Discs large in *Drosophila*, which are required for each other's localization and the control of general epithelial polarity[8]. The severe polarity defects caused by both *dlg* and *scrb* mutants have made it difficult to identify direct targets of Scribble and Discs large that are required for specific aspects of junctional integrity in *Drosophila*. The Protein 4.1 family member Coracle has been implicated as a possible target of Discs large. Coracle localizes to septate junctions and is required for maintaining the tightness of the paracellular space[11]. Although the protein is mislocalized in *dlg* mutants, no physical interaction of Discs large and Coracle has been observed; because Coracle localization probably requires proper apicobasal polarity of the junctions, regulation of Coracle by Discs large could be indirect[6,38]. Our demonstration that AJM-1 is a direct binding partner of DLG-1 that does not affect apicobasal polarity clarifies the role of proteins of the

Discs large family in regulating the structural integrity of epithelial junctions. A better understanding of the nature and function of the apical junctional domain to which DLG-1 and AJM-1 localize in *C. elegans* will require the identification of other binding partners for these proteins. This in turn should shed additional light on the function and regulation of epithelial junctions in general. □

Methods

Strains.
The Bristol strain N2 was used as the wild type and handled as described[39].

JJ1136 (*unc119(e2498::Tc1)*III; zvEx24(*unc119(+) hmp-1::gfp*) was a gift from James Priess. The strains BC2991 (*dpy-18(e364)/eT1* III; *dpy-11(e224) let-413(s128) unc-42(e270)/eT1* V) and BC2511 (*dpy-18(e364)/eT1* III; *unc-60(e677) dpy-11(e224) sDf35/eT1* V) were received from the *Caenorhabditis* Genetics Center.

ajm-1 cloning.
To identify the original *ajm-1* cDNA designated mh-1, a directional cDNA expression library of mixed-stage *C. elegans* was constructed in lgt11 (Promega Corp., Madison, Wisconsin) with the *Eco*RI–*Not*I restriction sites in accordance with the manufacturer's protocol. The original titre of this library was 4.8×10^6 plaque-forming units ml⁻¹, with 97% of the phage containing inserts ranging from 0.5 to 2.0 kb; the average size of insert was 1.2 kb. Clones obtained by screening the lgt11 cDNA library by DNA hybridization were digested with *Sfi*I and *Not*I, gel-purified and ligated to pGEM-11Zf digested with the same enzymes. RT–PCR was performed using Superscript II reagents (Gibco BRL, Rockville, Maryland). Poly(A)⁺ RNA from mixed-stage N2 animals was used as template for first-strand synthesis. SL-1 primer and a poly(T) primer were used for first-strand synthesis for the 5′ end and 3′ end, respectively. Exons 2 and 4 were shown to be alternative SL-1-*trans*-spliced transcription start sites. The third 5′ start site was identified by sequencing of the EST *yk285a2*; it extends into exon 1, which is contained in H08J11 (all Kohara cDNAs were gifts from Y. Kohara). One 3′ end was identified by sequencing of the ESTs *yk28c11* and *yk285a2*; both extend into a putative 3′ untranslated region (UTR) after exon 9. The second 3′ end was identified by sequencing of RT–PCR clones and the ESTs *yk344g1*, *yk161c3* and *yk152f7*; all clones extend into a putative 3′ UTR after exon 20. Northern blot analysis was performed essentially as described previously[40]. Poly(A)⁺ RNA of mixed-stage N2 worms was used and northern blots were probed with probes specific to exon 1, exons 5–8, the predicted 3′ UTR of exon 9, and exons 16–19. Northern sizes were in agreement with conceptual cDNAs derived from RT–PCR clones and sequenced ESTs (data not shown).

ajm-1 mutant isolation.
ajm-1(jc18) was isolated in a linked lethal screen. *unc-27* and *dpy-6* map within 0.5 map unit from the *ajm-1* gene locus on chromosome X; *unc-27(e155)/dpy-6(e14)* L4 animals were mutagenized with ethyl methyl sulphonate, and 5000 F₁ progeny were singled and screened for the absence of the *dpy-6* phenotype in the F₂ generation. Initial positives were re-screened for dead embryos and the remaining positives were tested for the absence of AJM-1 expression by staining with MH27. *ajm-1(ok160)* was isolated in a PCR-based deletion screen performed by the *C. elegans* Knockout Consortium in Oklahoma as described previously[41]. An external primer pair (5′-ACTATTTCGCACCTTGGCTC-3′ and 5′-ATAGTGATGACGGTGGG-3′) spanning 3.5 kb and a nested pair (5′-TACCGACCGAGAAGT-GATGAC-3′ and 5′-ACAGGAGTCATGCGGATTTC-3′) spanning 3.1 kb were used. The deletion breakpoints of *ajm-1(ok160)* on cosmid C25A11 are 6232 and 8598.

Electron microscopy.
For immuno-TEM of larvae with MH27, post-embedding immuno-TEM procedures were conducted on animals fixed in buffered aldehydes and embedded in LR Gold resin[42,43]. MH27 antibody (1/500 to 1/2000 dilution) was localized on thin sections on nickel mesh grids with gold-labelled secondary antibodies (AuroProbe; Amersham Life Science).

For analysis of hypodermal junctions in wild-type and *ajm-1* mutants, embryos were mounted on a thin agar pad and immobilized with low-melting-point gelatin agar under a coverslip. A small piece of agar containing the embryos was cut out of the mount and frozen at high pressure in a Balzer HPM high-pressure freezer. After freeze substitution in 2% OsO4, 1% uranyl acetate, samples were embedded in Epon and 40–100-nm sections were post-stained with uranyl acetate and lead citrate. Sections were viewed on a Philips CM 120 electron microscope at 60–80 kV accelerating voltage. For mutant analysis, a strain homozygous for *ajm-1(ok160)* and rescued by an extrachromosomal array containing *ajm-1::gfp* was used. Mutants were identified by confocal microscopy to score the loss of *ajm-1::gfp* and staged with Nomarski optics.

RNAi.
Templates for RNA synthesis for RNAi experiments were generated by PCR-amplifying cDNAs from pBluescript vector (Stratagene, La Jolla, California). Primers flanking T3 and T7 sites were used (5′-TTGTAAAACGACGGCCAG-3′ and 5′-CATGATTACGCCAAGCTC-3′) and transcription *in vitro* was performed with Ambion Megascript reagents (Ambion, Austin, Texas). *yk28c11* was used for *ajm-1(RNAi)*; *yk25e5* was used For *dlg-1(RNAi)* and *yk524b7* was used for *let-413(RNAi)*. In each case, double-stranded RNA at a concentration of 1–4 mg ml⁻¹ was injected into the body cavity of adult worms[32].

ajm-1::gfp and dlg-1::gfp expression analysis.
The *ajm-1::gfp* clone (pJS191) was constructed by cloning a bright mutant GFP (S65A, V68L, S72A) in frame into exon 8 of a genomic clone containing exons 2–9. Transgenic lines were generated with pRF4 (*rol(su1006)*)[44] as co-injection marker, and the array was integrated into chromosome IV of wild-type worms to create the integrated array *jcIs1* (strain SU93). *jcIs1* was crossed into the *ajm-1(ok160)* mutant background and shown to rescue mutants to viability. *jcIs1* was used to determine the AJM-1 expression pattern. To address the requirement of amino acids 102–204 for AJM-1 function, an oligonucleotide encoding stop codons in all reading frames was cloned into a *Bgl*II site in exon 3 of pJS191, essentially eliminating exon 2 as a transcription start and allowing expression only from exon 4. To generate a strain of nematodes expressing *dlg-1::gfp* using its own promoter (strain OR113), we created the free array *odEx33(dlg-1::gfp; rol(su1006))*. The plasmid CR16, a GFP translational fusion at the C terminus of genomic *dlg-1*, was made by cloning a 5-kb *Xho*I/*Apa*I fragment from the cosmid C25F6 into the GFP vector PD95.75 (Andy Fire). Live imaging of AJM-1–GFP and DLG-1–GFP was performed via automated time-lapse multiphoton laser scanning microscopy, essentially as described previously[13]. Three-dimensional stacks containing slices spaced 1 μm apart were taken every 5 min over several hours. Z-projections of the stacks were done with NIH Image software.

Antibodies and immunostaining.
Antibody staining of embryos was performed with the freeze-cracking method essentially as described previously[18]. The following primary antibodies were used at the dilutions indicated: MH27 at 1:500 and MH46 at 1:100 (gifts from R. Waterston), R224 at 1:100 (a gift from A. Kagawa), anti-HMP-1 at 1:100 (a gift from J. Priess) anti-DLG at 1:3000 (gift from V. Budnik), anti-PAR-3 at 1:40 and anti-PAR-6 at 1:20 (gifts from K. Kemphues), anti-SMA-1 at 1:125 (a gift from J. Austin) and anti-UNC-70 at 1:500 (a gift from V. Bennett). Phalloidin staining was performed as previously described[18]. Images were captured on a Bio-Rad MRC1024 confocal microscope.

Yeast two-hybrid analysis.
The yeast two hybrid-screen was performed with yeast strain L40ura– as previously described[45]. In brief, the pLexA–AJM-1 plasmid was constructed with a partial *ajm-1* cDNA encoding amino acids 180–809. L40ura– yeast cells containing this plasmid were transformed with a random-primed cDNA library, LambdaACT-RB-2. The library transformation was plated on SD-Trp-Leu-His plates containing 5 mM 3-aminotriazole. Colonies were picked after 6 days and tested for reporter (*lacZ*) expression. The cDNA-containing plasmids of those testing positive were recovered and sequenced. The specificity of the interactions was addressed in directed assays by introducing pLexA–AJM-1 into L40 together with recovered cDNA plasmids, and for negative controls, with the empty pGal4 (Gal4 activation domain) plasmid alone or pGal4–IRP (Iron Response Protein). In each case, *lacZ* expression was assayed in triplicate using a X-Gal colony filter assay as described previously[45]. In directed two-hybrid tests, pBTMKnDB and pACT2 were used as vectors for the LexA and Gal4 activation domain (Gal4) plasmids, respectively (gifts from M. Wickens).

GST pull-down assay.
The GST–DLG-1 fusion was generated by cloning *dlg-1* cDNA (encoding amino acids 28–483) into pGEX-5X-1 and introduced into the *E. coli* strain BL21(DE3) (Stratagene, La Jolla, CA). GST was generated using empty pGEX-5X-1. Bacteria were grown in TB plus 2% Glucose to log phase at 37°C, induced with 0.1 mM isopropylthiogalactoside for 2 h at 25 °C and harvested. Cells were lysed with B-PER reagent (Pierce, Rockford, Illinois), with Complete protease inhibitor cocktail (Boehringer-Mannheim, Indianapolis, Indiana), in accordance with the manufacturers' directions. Recombinant protein was bound to glutathione–Sepharose beads (Amersham Pharmacia Biotech, Piscataway, New Jersey) and repeatedly washed with buffer A (20 mM Tris-HCl pH 7.9, 0.2 mM EDTA, 0.1 M NaCl, 1 mM dithiothreitol, 0.2% Nonidet P40, and Complete protease inhibitor cocktail). Radiolabelled AJM-1 protein (amino acids 1–868) was generated by *in vitro* translation with the TNT Coupled Reticulocyte Lysate System (Promega). The Kohara clone *yk285a2* was used as template. For the protein binding assays *in vitro*, labelled AJM-1 was added to equivalent quantities of beads carrying GST–DLG-1 or GST alone. The quantities of coupled protein were similar for each protein, as judged by staining of the proteins after SDS–PAGE. Radiolabelled protein was incubated with beads in buffer A at 4 °C, with rocking. Beads were pelleted, washed four times in buffer A and eluted by boiling in SDS–PAGE sample buffer. Eluted labelled protein was analysed by SDS–PAGE. An equivalent of 20% of the labelled AJM-1 used in the binding assays was run as a comparison.

1. Gumbiner, B. M. Cell adhesion: the molecular basis of tissue architecture and morphogenesis. *Cell* **84**, 345–357 (1996).
2. Tepass, U. Genetic analysis of cadherin function in animal morphogenesis. *Curr. Opin. Cell Biol.* **11**, 540–548 (1999).
3. Willott, E. *et al.* The tight junction protein ZO-1 is homologous to the *Drosophila* discs-large tumor suppressor protein of septate junctions. *Proc. Natl Acad. Sci. USA* **90**, 7834–7838 (1993).
4. Woods, D. F. & Bryant, P. J. ZO-1, DlgA and PSD-95/SAP90: homologous proteins in tight, septate and synaptic cell junctions. *Mech. Dev.* **44**, 85–89 (1993).
5. Tsukita, S., Furuse, M. & Itoh, M. Structural and signalling molecules come together at tight junctions. *Curr. Opin. Cell Biol.* **11**, 628–633 (1999).
6. Woods, D. F., Hough, C., Peel, D., Callaini, G. & Bryant, P. J. Dlg protein is required for junction structure, cell polarity, and proliferation control in *Drosophila* epithelia. *J. Cell Biol.* **134**, 1469–1482 (1996).
7. Hough, C. D., Woods, D. F., Park, S. & Bryant, P. J. Organizing a functional junctional complex requires specific domains of the *Drosophila* MAGUK Discs large. *Genes Dev.* **11**, 3242–3253 (1997).
8. Bilder, D., Li, M. & Perrimon, N. Cooperative regulation of cell polarity and growth by *Drosophila* tumor suppressors. *Science* **289**, 113–116 (2000).
9. Legouis, R. *et al.* LET-413 is a basolateral protein required for the assembly of adherens junctions in *Caenorhabditis elegans. Nature Cell Biol.* **2**, 415–422 (2000).
10. Baumgartner, S. *et al.* A *Drosophila* neurexin is required for septate junction and blood–nerve barrier formation and function. *Cell* **87**, 1059–1068 (1996).
11. Lamb, R. S., Ward, R. E., Schweizer, L. & Fehon, R. G. Drosophila coracle, a member of the protein 4.1 superfamily, has essential structural functions in the septate junctions and developmental functions in embryonic and adult epithelial cells. *Mol. Biol. Cell* **9**, 3505–3519 (1998).

12. Bilder, D. & Perrimon, N. Localization of apical epithelial determinants by the basolateral PDZ protein Scribble. *Nature* **403**, 676–680 (2000).
13. Mohler, W. A., Simske, J. S., Williams-Masson, E. M., Hardin, J. D. & White, J. G. Dynamics and ultrastructure of developmental cell fusions in the *Caenorhabditis elegans* hypodermis. *Curr. Biol.* **8**, 1087–1090 (1998).
14. Raich, W. B., Agbunag, C. & Hardin, J. Rapid epithelial-sheet sealing in the *Caenorhabditis elegans* embryo requires cadherin-dependent filopodial priming. *Curr. Biol.* **9**, 1139–1146 (1999).
15. Francis, R. & Waterston, R. H. Muscle cell attachment in *Caenorhabditis elegans*. *J. Cell Biol.* **114**, 465–479 (1991).
16. Podbilewicz, B. & White, J. G. Cell fusions in the developing epithelial of *C. elegans*. *Dev. Biol.* **161**, 408–424 (1994).
17. Priess, J. R. & Hirsh, D. I. *Caenorhabditis elegans* morphogenesis: the role of the cytoskeleton in elongation of the embryo. *Dev. Biol.* **117**, 156–173 (1986).
18. Williams-Masson, E. M., Malik, A. N. & Hardin, J. An actin-mediated two-step mechanism is required for ventral enclosure of the *C. elegans* hypodermis. *Development* **124**, 2889–2901 (1997).
19. Costa, M. *et al.* A putative catenin–cadherin system mediates morphogenesis of the *Caenorhabditis elegans* embryo. *J. Cell Biol.* **141**, 297–308 (1998).
20. Waterston, R. H. The minor myosin heavy chain, mhcA, of *Caenorhabditis elegans* is necessary for the initiation of thick filament assembly. *EMBO J.* **8**, 3429–3436 (1989).
21. Gatewood, B. K. & Bucher, E. A. The *mup-4* locus in *Caenorhabditis elegans* is essential for hypodermal integrity, organismal morphogenesis and embryonic body wall muscle position. *Genetics* **146**, 165–183 (1997).
22. Kagawa, H. & Gengyo, K. Antigenic sites of the muscle protein, paramyosin, in *Caenorhabditis elegans* determined with exon-expression plasmid. *Nucleic Acids Symp. Ser.* **19**, 81–84 (1988).
23. Williams, B. D. & Waterston, R. H. Genes critical for muscle development and function in *Caenorhabditis elegans* identified through lethal mutations. *J. Cell Biol.* **124**, 475–490 (1994).
24. Moorthy, S., Chen, L. & Bennett, V. *Caenorhabditis elegans* β-G spectrin is dispensable for establishment of epithelial polarity, but essential for muscular and neuronal function. *J. Cell Biol.* **149**, 915–930 (2000).
25. Hresko, M. C., Williams, B. D. & Waterston, R. H. Assembly of body wall muscle and muscle cell attachment structures in *Caenorhabditis elegans*. *J. Cell Biol.* **124**, 491–506 (1994).
26. Woods, D. F. & Bryant, P. J. The discs-large tumor suppressor gene of *Drosophila* encodes a guanylate kinase homolog localized at septate junctions. *Cell* **66**, 451–464 (1991).
27. Bossinger, O., Klebes, A., Segbert, C., Theres, C. & Knust, E. Zonula adherens formation in *Caenorhabditis elegans* requires *dlg-1*, the homologue of the *Drosophila* gene discs large. *Dev. Biol.* **230**, 29–42 (2001).
28. Itoh, M. *et al.* Direct binding of three tight junction-associated MAGUKs, ZO-1, ZO-2, and ZO-3, with the COOH termini of claudins. *J. Cell Biol.* **147**, 1351–1363 (1999).
29. Songyang, Z. *et al.* Recognition of unique carboxyl-terminal motifs by distinct PDZ domains. *Science* **275**, 73–77 (1997).
30. Cordenonsi, M. *et al.* Cingulin contains globular and coiled-coil domains and interacts with ZO-1, ZO-2, ZO-3, and myosin. *J. Cell Biol.* **147**, 1569–1582 (1999).
31. Koh, Y. H., Popova, E., Thomas, U., Griffith, L. C. & Budnik, V. Regulation of DLG localization at synapses by CaMKII-dependent phosphorylation. *Cell* **98**, 353–363 (1999).
32. Fire, A. *et al.* Potent and specific genetic interference by double-stranded RNA in *Caenorhabditis elegans*. *Nature* **391**, 806–811 (1998).
33. Rothnagel, J. A. & Rogers, G. E. Trichohyalin, an intermediate filament-associated protein of the hair follicle. *J. Cell Biol.* **102**, 1419–1429 (1986).
34. Matsumura, F. & Yamashiro, S. Caldesmon. *Curr. Opin. Cell Biol.* **5**, 70–76 (1993).
35. Svitkina, T. M., Verkhovsky, A. B. & Borisy, G. G. Plectin sidearms mediate interaction of intermediate filaments with microtubules and other components of the cytoskeleton. *J. Cell Biol.* **135**, 991–1007 (1996).
36. Cordenonsi, M. *et al. Xenopus laevis* occludin. Identification of in vitro phosphorylation sites by protein kinase CK2 and association with cingulin. *Eur. J. Biochem.* **264**, 374–384 (1999).
37. Nusrat, A. *et al.* The coiled-coil domain of occludin can act to organize structural and functional elements of the epithelial tight junction. *J. Biol. Chem.* **275**, 29816–29822 (2000).
38. Ward, R. E. 4th, Lamb, R. S. & Fehon, R. G. A conserved functional domain of *Drosophila* coracle is required for localization at the septate junction and has membrane-organizing activity. *J. Cell Biol.* **140**, 1463–1473 (1998).
39. Brenner, S. The genetics of *Caenorhabditis elegans. Genetics* **77**, 71–94 (1974).
40. Sambrook, J., Fritsch, E. F. & Maniatis, T. *Molecular Cloning, A Laboratory Manual* (Cold Spring Harbor Laboratory, Cold Spring Harbor, New York, 1989).
41. Dernburg, A. F. *et al.* Meiotic recombination in *C. elegans* initiates by a conserved mechanism and is dispensable for homologous chromosome synapsis. *Cell* **94**, 387–398 (1998).
42. Selkirk, M. E., Gregory, W. F., Yazdanbakhsh, M., Jenkins, R. E. & Maizels, R. M. Cuticular localisation and turnover of the major surface glycoprotein (gp29) of adult *Brugia malayi. Mol. Biochem. Parasitol.* **42**, 31–43 (1990).
43. Hall, D. H. Electron microscopy and three-dimensional image reconstruction. *Methods Cell Biol.* **48**, 395–436 (1995).
44. Mello, C. & Fire, A. DNA transformation. *Methods Cell Biol.* **48**, 451–482 (1995).
45. Bartel, P. L. & Fields, S. *The Yeast Two-hybrid System* (Oxford Univ. Press, New York, 1997).